Impacts of Hot Space Plasma and Ion Beam Emission on Electrostatic Tractor Performance

Erik A. Hogan and Hanspeter Schaub

***Abstract*— A recent proposed technique for geostationary debris mitigation is the electrostatic tractor. The tug vehicle approaches a debris object to within 20 m and emits a focused electron beam onto it. This results in a negative charge on the debris and a positive charge on the tug vehicle. Used in conjunction with low thrust, the electrostatic force is used to tow a debris object into a disposal orbit. In this paper, the impacts of geomagnetic storm activity on the charging of tug and debris are considered. The influence of electrons emitted from the debris (photoelectrons and secondary electrons) on tug charging is also considered. Both of these phenomena yield improved electrostatic tractor performance. The simultaneous emission of an electron and ion beam by the tug is also considered to improve tractor performance and enable charge transfer for scenarios where it fails when only an electron beam is used. The theoretical maximum electrostatic force that is possible with simultaneous emission is computed, and the results indicate that emitting both an electron and ion beam enables smaller tug vehicles to tow larger objects that could not otherwise be towed with only an electron beam.**

***Index Terms*— Electrostatic tractor, geomagnetic storm impacts on charging, spacecraft charge control.**

I. Introduction

THE high value of the geostationary (GEO) ring, coupled with the increasing number of orbital debris, highlights the need for active debris removal methods [1]–[3]. When spacecraft reach end of life in GEO, international guidelines call for reorbiting into a disposal orbit typically 200–300 km above GEO [4], [5]. For debris objects that do not possess the ability for reorbiting, an external method is needed to reach the disposal orbit. Originally proposed as a means for asteroid deflection [6], the electrostatic tractor has been suggested as a means for GEO debris remediation [7]. The concept relies on a combination of an attractive electrostatic force between two craft and low thrusting capability on one of the craft, as shown in Fig. 1. The attractive force acts as a virtual tether between the two objects, and a low thrust maneuver is used to tow the noncooperative, possibly tumbling large debris object into a new orbit [8]. GEO debris can be tumbling up to tens of degrees per second [9], making any physical docking methods particularly challenging [10]. The electrostatic tractor method allows the tumbling object to be reorbited without first having to despin it. Considering nonsymmetrical spacecraft geometries, the charging also gives rise to torques on the craft [11]–[13]. Through careful manipulation of the charging histories, these torques can be applied in a manner sufficient to despin a noncooperative object remotely [12]. This latter ability greatly simplifies any orbital servicing mission where great efforts are required to first despin objects spinning at 1°/s or greater [10], [14].

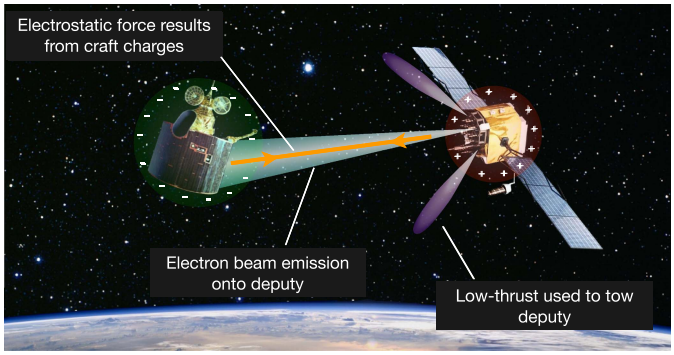

Fig. 1. Illustration of electrostatic tractor concept.

For the electrostatic tractor application, a method of active charge control is needed. Charged particle beams are the most ideal candidates for this purpose. Emitting a high-energy beam (tens of kiloelectronvolts) at sufficient current levels enables the tug to reach high potentials. Either an ion or electron beam may be used though an electron beam is preferred due to its simpler implementation and reduced momentum transfer [12]. Directing the beam onto the debris provides a current that will affect the debris charging, much like the natural charging that occurs due to the plasma environment. The vast majority of prior work with Coulomb formations merely assume either a charge or a potential on the different spacecraft in the formation, without actually modeling the mechanism for and environmental influences on achieving the charging [8], [12], [15]–[20]. The electrostatic tractor performance is dependent on the charging that is achieved with electron or ion beam emission, and it is important to characterize the charge transfer process. Reference [12] presents a first-order charging model to compute potentials on tug and debris as a function of various environmental current sources applied to the electrostatic tractor problem. Assuming an electron beam is used for charge control, one particular tug and debris configuration is considered, and the resulting electrostatic forces are computed for specific space weather conditions. The work does not consider the impact of solar

Manuscript received August 14, 2014; revised February 1, 2015, May 24, 2015, and June 22, 2015; accepted June 24, 2015. Date of publication July 24, 2015; date of current version September 9, 2015.

The authors are with the Colorado Center for Astrodynamics Research, University of Colorado Boulder, Boulder, CO 80309 USA (e-mail: erik.hogan@colorado.edu; hanspeter.schaub@colorado.edu).

Color versions of one or more of the figures in this paper are available online at http://ieeexplore.ieee.org.

Digital Object Identifier 10.1109/TPS.2015.2451001

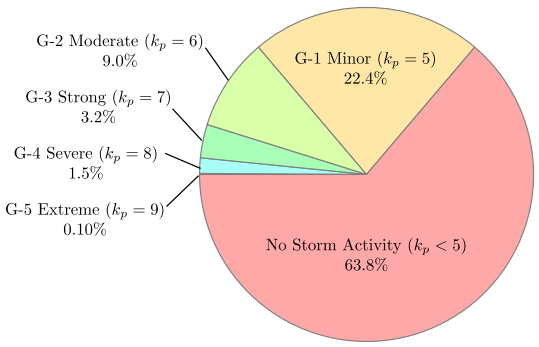

Fig. 2. Percent of days in an 11-year solar cycle for which various geomagnetic storm levels occur (data adapted from [26]).

storm events on tractor performance or the simultaneous use of electron and ion beam emissions for improved performance. This first-order charging model provides the tools needed to analyze general charging trends that may be encountered for the electrostatic tractor application, and is extensively used in the current study.

The charging of a spacecraft is dependent on the space plasma environment [21], [22]. Because of the potential threats to mission viability caused by charging events, much work has been done to characterize the space weather environment both in low earth orbit (LEO) and GEO [23], [24]. The plasma environment is typically characterized by two parameters: 1) density and 2) temperature. The LEO plasma environment is much colder and denser than in GEO, with typical LEO densities ranging from 10^4 to 10^6 particles/cm^{-3} and corresponding temperatures below 1 eV. In GEO, the plasma densities are orders of magnitude smaller, ranging from 0.1–10 particles/cm^{-3}. Depending on geomagnetic storm activity, ion temperatures may range from below 100 to 20 keV or more. Electron temperatures are typically above 1 keV and may reach tens of kiloelectronvolts depending on storm activity.

The severity of geomagnetic storms is classified using the K_p index, which is based on the observed variation in the degree of irregular magnetic activity throughout each day, observed at various ground stations [25]. The K_p index utilizes an integer scale ranging from 0 to 9, and values of 5 and up indicate that a geomagnetic storm is occurring. The National Oceanic and Atmospheric Administration (NOAA) has also developed a scale for classifying the severity of geomagnetic storms [26]. The scale ranges from G-1 minor storms ($K_p = 5$) to G-5 extreme storms ($K_p = 9$). The NOAA scale provides information about expected impacts to spacecraft for different storm levels. In a minor storm (G-1, $K_p = 5$), minimal impacts to spacecraft operations can be expected. At the other end of the spectrum, an extreme storm (G-5, $K_p = 9$) may cause extensive surface charging, loss of attitude, and problems with communications and satellite tracking [27]. Fortunately, stronger storms only occur a few times per 11-year solar cycle. The frequency of occurrence for the various storm conditions in a typical solar cycle is shown in Fig. 2. The vast majority of the time (>85%), there is either no storm activity or a minor storm occurrence. In addition to solar storms, more frequent geomagnetic substorms provide additional local sources of hot plasma to the GEO environment [28].

In prior work, considering environmental impacts on electrostatic tractor performance, quiet storm conditions are used [29]. Further, only electron beam emission is considered as a means for charge control [12], [29]. Reference [30] illustrates that when the debris sizes are roughly the same as or larger than the tug, it becomes very difficult for charge transfer to occur when only an electron beam is used. As the debris object becomes larger, more incoming electron beam current is needed to offset the higher amounts of photoelectrons emitted from the debris. If the tug vehicle is smaller than the debris, it will maximally charge itself to the point that emitted beam electrons are recaptured before it can deliver enough current to the debris to initiate debris charging. In this paper, several novel results are presented. First, the impacts of geomagnetic storm and substorm events on the charge transfer process are considered. These storm events lead to changes in the plasma environment in GEO, and change the charging behavior of the tug and debris. While there is a large variability in GEO plasma conditions, the purpose of this paper is to identify a few representative conditions typical of solar storm and substorm events and identify how the resulting hot plasma affects the charge transfer process between tug and debris. To mitigate some of the relative sizing issues, simultaneous emission of an electron beam (onto the debris) and an ion beam (into space) is considered as a means to improve charge transfer performance by providing an additional control variable for charge control. It is shown that there are potentials on tug and debris that yield the maximum possible electrostatic force and different environmental currents throw off this balance. Ion beam emission is explored as a means to offset these effects and move the potentials toward the optimal values. During charging, electrons are emitted from the debris surface. In the vicinity of the positively charged tug, some of these electrons will be recaptured. This back flux has thus far not been investigated. In this paper, the impacts of this electron back flux onto the tug on tractor performance are investigated as well.

This paper is structured as follows. First, an overview of the charging and electrostatic force models is presented. Next, the influence of geomagnetic storm conditions on charging is presented and compared with quiet storm conditions. Then, the effects of the electron back flux from debris to tug on tractor performance are investigated. Finally, the simultaneous emission of an electron and ion beam is considered, and the performance benefits that result are characterized.

II. Background

A. Charge Transfer Model

The electrostatic tugging force used for towing is dependent on the charging that occurs on both the tug and debris. Several factors influence this charging process. Naturally occurring ion and electron plasma currents are collected by the spacecraft, and photoelectrons may be emitted depending on the spacecraft potential and presence of sunlight. Focused electron beam emission by the tug is used for charge control. When the electron beam is absorbed by the debris, secondary electron emission occurs as the incoming beam electrons excite and release electrons from the debris surface material.

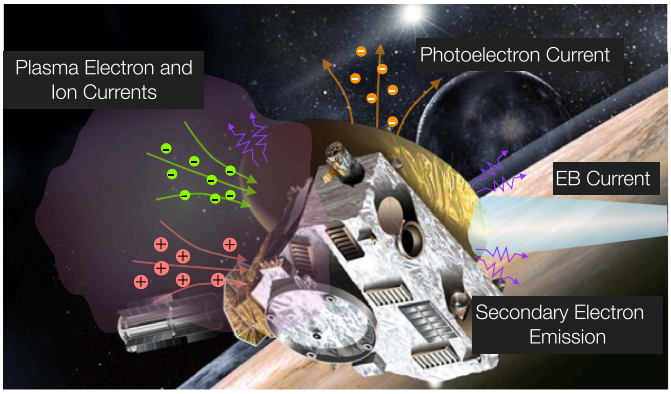

Fig. 3. Illustration of various current sources that affect spacecraft charging.

The potential levels achieved by the tug and debris result from a balance of these various current sources, which are shown in Fig. 3. To compute these potentials, the charging model developed in [31] is applied. The model is repeated below to aid the reader.

A photoelectron current occurs whenever the spacecraft are in sunlight. This current is modeled as [21]

$$I_{\rm ph}(\phi) = j_{\rm ph,0} A_\perp e^{-q\phi/k_B T_{\rm ph}}, \quad \phi > 0 \tag{1a}$$
$$= j_{\rm ph,0} A_\perp, \quad \phi \le 0 \tag{1b}$$

where ϕ is the spacecraft potential, $T_{\rm ph} = 2$ eV is the temperature of the emitted photoelectrons, $j_{\rm ph,0} = 20\ \mu{\rm A/m}^2$ is the photoelectron current density, k_B is the Boltzmann constant, and $A_\perp$ is the cross-sectional area exposed to sunlight. For the spherical geometries assumed here, $A_\perp = \pi r^2$. For high positive potentials, the photoelectron current is effectively zero because all of the emitted electrons are recaptured.

The plasma electron current is modeled as [32]

$$I_e(\phi) = -\frac{Aqn_e w_e}{4} e^{q\phi/k_B T_e}, \quad \phi < 0 \tag{2a}$$
$$= -\frac{Aqn_e w_e}{4}\left(1 + \frac{q\phi}{k_B T_e}\right), \quad \phi \ge 0 \tag{2b}$$

where A is the surface area exposed to the plasma environment, T_e is the plasma electron temperature, n_e is the plasma electron density, q is the unsigned elementary charge, and $w_e = (8k_B T_e/\pi m_e)^{1/2}$ is the thermal velocity of the electrons. The electron mass is represented by m_e. Note that for large negative potentials, I_e is very small. This is due to the fact that electrons are repelled by the negatively charged spacecraft. Similarly, the plasma ion current is computed using [32]

$$I_i(\phi) = \frac{Aqn_i w_i}{4} e^{-q\phi/k_B T_i}, \quad \phi > 0 \tag{3a}$$
$$= \frac{Aqn_i w_i}{4}\left(1 - \frac{q\phi}{k_B T_i}\right), \quad \phi \le 0 \tag{3b}$$

where $w_i = (8k_B T_i/\pi m_i)^{1/2}$. Note that the variable quantities represent the same parameters as before, except the subscript i is used to denote they represent ions. In the space weather model for the GEO environment utilized here, the ion species consists solely of protons. For high positive potentials, the ion current is very small because the ions are repelled by the positively charged spacecraft.

Charge control is achieved using an electron beam emitted from the tug onto the debris. A portion of the beam current will be absorbed by the debris, depending on tug pointing accuracy and the charge levels of both tug and debris. This current is modeled as

$$I_D(\phi_D, \phi_T) = -\alpha I_t q\phi_T - q, \quad \phi_D < E_{\rm EB} \tag{4a}$$
$$= 0q\phi_T - q, \quad \phi_D \ge E_{\rm EB} \tag{4b}$$

where I_t is the beam current emitted by the tug, $E_{\rm EB}$ is the electron beam energy, and the subscripts T and D represent the tug and debris, respectively. The parameter α represents the efficiency of the charge transfer process; it is the fraction of the beam current emitted by the tug that reaches the debris. In general, this is a function of beam pointing accuracy and any spreading of the beam that results from the tug and debris potentials relative to the beam energy level. In this paper, a value of $\alpha = 1$ is used, which maintains the value established in [31]. This assumes a well focused and accurately pointed beam. Better quantification of the α parameter is beyond the scope of this paper and is left for future work. While beam electrons are unable to reach the deputy once the tug–deputy potential difference reaches the beam energy, in general, the potential difference between tug and debris will not approach the beam energy due to losses that result from environmental current sources and secondary electron emission. It is not clear whether or not this potential difference is high enough to cause sufficient beam spreading to affect the charging performance. Investigation of this phenomenon is suggested as an avenue for future research.

When the electron beam impacts the debris object, the incoming electrons result in the emission of secondary electrons. Because of the large negative potential of the debris object (kilovolt level), these electrons will escape. This represents a significant current source that must be accounted for. Secondary electron emission is modeled as [33]

$$I_{\rm SEE}(\phi_D, \phi_T) = -4Y_M I_D(\phi_D, \phi_T)\kappa, \quad \phi_D < 0 \tag{5a}$$
$$= 0, \quad \phi_D \ge 0 \tag{5b}$$

where

$$\kappa = \frac{E_{\rm eff}/E_{\rm max}}{(1 + E_{\rm eff}/E_{\rm max})^2} \tag{6}$$

and $E_{\rm eff} = E_{\rm EB} - q\phi_T + q\phi_D$. Y_M is the maximum yield of secondary electron production and $E_{\rm max}$ is the impact energy at which this maximum occurs. In this paper, the values of $Y_M = 2$ and $E_{\rm max} = 300$ eV are used.

The tug settles to a potential that satisfies the current balance

$$I_e(\phi_T) + I_t + I_i(\phi_T) + I_{\rm SEE}(\phi_D, \phi_T) + I_{\rm ph}(\phi_T) = 0.$$

Because the tug achieves a high positive potential, the majority of its emitted secondary electrons and photoelectrons are recaptured. Furthermore, the plasma ion current is minimal, because the ions are repelled by the tug. Thus, the current balance on the tug is approximated by

$$I_e(\phi_T) + I_t = 0. \tag{7}$$

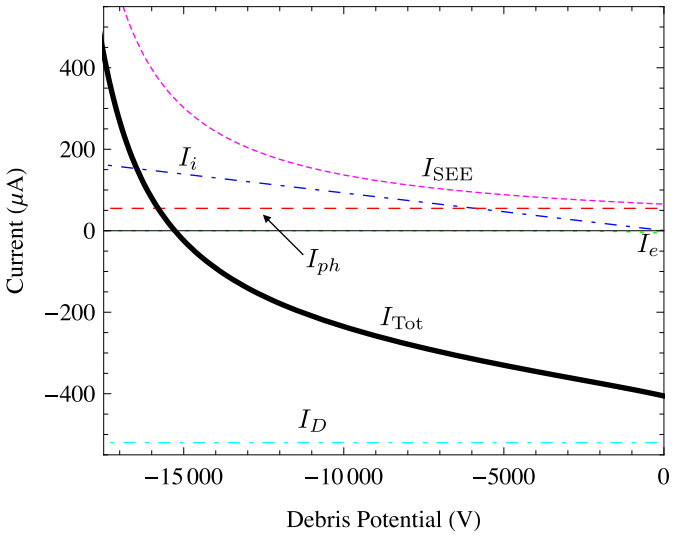

Fig. 4. Currents acting on the debris for a range of debris potentials, generated from (9). Debris achieves a potential that results in $I_{\text{Tot}} = 0$.

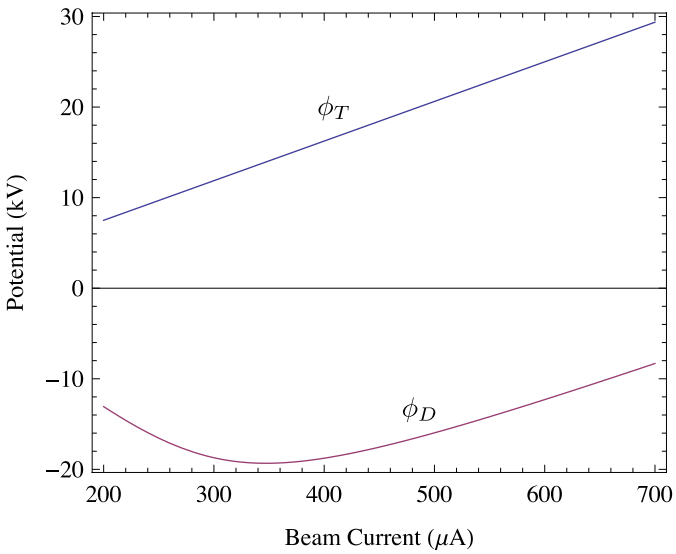

Fig. 5. Tug and debris potentials as a function of beam current, generated using (7) and (9).

This is solved analytically as

$$\phi_T = \left(\frac{4I_t}{Aqn_e w_e} - 1\right)\frac{k_B T_e}{q} \tag{8}$$

which assumes a positive tug potential. This will be the case provided the beam current is sufficient. The current balance on the debris object contains a few more contributions, and an analytical solution does not exist. The debris will achieve a potential that satisfies

$$\begin{aligned} I_{\text{Tot}} = {} & I_e(\phi_D) + I_i(\phi_D) + I_{\text{SEE}}(\phi_D, \phi_T) \\ & + I_{\text{ph}}(\phi_D) + I_D(\phi_D, \phi_T) = 0. \end{aligned} \tag{9}$$

The presence of the photoelectron current implies the debris is in the sunlight. When in the earth's shadow, the current balance contains all of the same terms except for I_{ph}. A numerical root finder is used to solve for ϕ_D in (9).

An example charging scenario is presented in Fig. 4. Shown are the various currents impacting debris charging for space weather conditions of $n_e = 0.6$ cm^{-3}, $n_i = 9.5$ cm^{-3}, $T_i = 50$ eV, and $T_e = 1250$ eV. The results assume a beam energy of $E_{\text{EB}} = 40$ keV and a beam current emitted from the tug of $I_t = 520$ μA. The tug and debris are treated as spheres, with radii of $r_T = 2$ m and $r_D = 0.935$ m. With these conditions, the tug achieves a potential of $\phi_T = 21.5$ kV and the debris reaches a potential of $\phi_D = -15.3$ kV. As observed in Fig. 4, the debris potential results in a net zero current balance, i.e., $I_{\text{Tot}} = 0$. While the plasma electron current is included in the current balance, for the debris, it provides an insignificant contribution to charging at the high potential levels achieved. The tug and debris potentials as a function of beam current are shown in Fig. 5. The tug potential linearly increases with beam current, while the debris potential has its largest value around $I_t = 350$ μA.

There are two electron beam parameters that may be used to influence charging: 1) the beam energy and 2) potential. In general, a higher beam energy will result in higher debris charging. This is due to the reduced secondary electron emission that stems from the higher energy of the incoming beam electrons. As the energy of an absorbed electron increases, fewer secondary electrons are emitted. Because the secondary electrons essentially result in the loss of some fraction of the incoming beam current, reducing the number of secondary electrons emitted will improve debris charging. Depending on the space weather conditions, increasing or decreasing the beam current can improve or worsen debris charging, as shown in Fig. 5. However, the tug will always charge to higher positive potentials as the beam current is increased, up to the level of the beam energy ($q\phi_T \leq E_{\text{EB}}$).

B. Electrostatic Force Model

The performance of the electrostatic tug is dependent on the electrostatic force in place between the tug and debris. To allow for analytic expressions, the tug and debris object are geometrically treated as spheres and are assumed to be perfectly conducting. The potential on the tug object is a result of its own charge and the potential due to the charged debris object as [18]

$$\phi_T = k_c\frac{q_T}{r_T} + k_c\frac{q_D}{\rho} \tag{10}$$

where $k_c = 8.99 \times 10^9$ Nm^2/C^2 is the Coulomb constant, ρ is the distance between tug and debris, q_T is the charge on the tug, q_D is the charge on the debris, and r_T is the radius of the tug craft. Similarly, the potential on the debris object is computed as

$$\phi_D = k_c\frac{q_D}{r_D} + k_c\frac{q_T}{\rho} \tag{11}$$

where r_D is the radius of the debris object.

If the potentials on the tug and debris are controlled, then the above relationships may be rearranged to solve for charge [18]

$$\begin{bmatrix} q_T \\ q_D \end{bmatrix} = \frac{\rho}{k_c(\rho^2 - r_T r_D)}\begin{bmatrix} r_T\rho & -r_T r_D \\ -r_T r_D & r_D\rho \end{bmatrix}\begin{bmatrix} \phi_T \\ \phi_D \end{bmatrix}. \tag{12}$$

After computing the charges, the electrostatic force between tug and debris is computed using

$$F_c = k_c \frac{q_T q_D}{\rho^2}. \tag{13}$$

Due to the space plasma environment, some shielding of this electrostatic force will occur. The distance over which this shielding is prevalent is described by the Debye length of the local plasma [34]. The space weather conditions considered in this study yield Debye lengths that are on the order of tens of meters. Reference [6] introduces the effective Debye length formalism to approximate the electrostatic force with partial plasma shielding when the object's potential is large compared with the plasma's energy level. This effective Debye length is similar to the true plasma-sheath distance.

Looking specifically at this phenomenon as it pertains to charging of meter sized objects in quiet GEO space weather conditions, the effective Debye lengths are predicted to be roughly five times larger than the classic Debye shielding model predicts ($\alpha \approx 5$) [35]. The shortest Debye lengths considered here are on the order of 15 m or more, leading to effective Debye lengths over 75 m. This implies that Debye shielding will not have a significant effect on the electrostatic force below distances of 75 m. Because the separation distances considered here are less than 20 m, the impacts of Debye shielding are insignificant and will not be included in the force model. Thus, (13) is used to compute the electrostatic forces presented in this paper.

The ultimate goal of the electrostatic tractor is to raise the debris orbit enough to reach a disposal orbit. The size of the debris orbit is characterized by its semimajor axis, and reaching a disposal orbit requires an increase in the debris semimajor axis of 200–300 km. Assuming a circular debris orbit, the semimajor axis increase in the debris orbit over one day is [7]

$$\Delta a \approx \frac{4\pi}{n^2} \frac{F_c}{m_D} \tag{14}$$

where n is the mean motion of the debris orbit and m_D the debris mass. A GEO orbit radius of 42 164 km is assumed for this analysis. The debris mass is required to compute the semimajor axis change. Considering publicly available data on GEO satellites, [18] provides a relationship between spacecraft mass and an approximate sphere radius. The simple linear expression

$$r_D(m_D) = 1.152 \text{ m} + 0.00066350 \frac{\text{m}}{\text{kg}} m_D \tag{15}$$

provides a debris radius for use in the charging model. While certainly not perfect, this linear relationship does capture the general trend of increased mass for larger objects and is based on actual data for GEO objects.

As an example of expected tractor performance, consider a scenario where a 2000 kg object is to be reorbited. The radius of the tug vehicle is assumed to be 2 m at a separation distance of 15 m from the debris object, with the tug at +20 kV and the debris at −15 kV. Equation (14) predicts that under these conditions, a debris semimajor axis increase of 1.2 km/day is expected.

III. Impact of Geomagnetic Storm Events on Tractor Performance

In [29], electrostatic tractor performance is analyzed for quiet ($K_p = 1.5$) geomagnetic storm conditions. Here, the effects of geomagnetic storm events are considered. When a geomagnetic storm occurs, the population of lower energy ions (1–100 eV) in the period following local midnight is lost, with a higher energy population of slightly lower density (1 cm^{-3}) remaining [24], [36]. Solar storm events also provide a higher energy population of electrons, with energies as high as a few tens of kiloelectron-volt. This phenomenon was experienced by the ATS-5 satellite and recorded in GEO space weather measurements taken by the magnetospheric plasma analyzer instruments flown by Los Alamos National Laboratory [37]. When a spacecraft enters into eclipse during a storm event, it may naturally charge to potential levels in excess of −10 kV, depending on the severity of the geomagnetic storm. During storm events experienced by ATS-5, typical potentials achieved in shadow were 3–4 kV (negative polarity), with lows of 70–100 V and highs in above 10 kV [36]. Note that a spacecraft experiences eclipse for under an hour each day in the 3–4 weeks before and after an equinox. Over an electrostatic tractor reorbiting scenario with a total transfer time of several months, this represents a very small portion of the total operating time. When a spacecraft is in the sunlight, the resulting photoelectron current helps to limit the natural charging somewhat, though relatively high potentials have been observed. ATS-5 observed a maximum potential of −300 V in the sunlight, and reached potentials of between −50 and −300 V several times. All of these charging events occurred during periods of very high solar activity and occurred between local midnight and dawn. The SCATHA satellite was also used to study natural charging in sunlight and recorded potentials as high as −740 V [38]. Charging events in excess of −100 V occurred only for K_p indices of 2 or greater.

The NOAA space weather scale classifies the severity and frequency of geomagnetic storms, with a scale ranging from G-1 (minor, $K_p = 5$) to G-5 (extreme, $K_p = 9$) [26]. In an 11-year solar cycle, minor storm activity is expected for roughly 900 days, with extreme storm events occurring much less frequently, only about four times. For the analysis of storm activity, two storm conditions are considered: 1) a moderate geomagnetic storm, G-2 on the NOAA scale, with $K_p = 6$ and 2) a worst-case severe storm event. Only the effects on the charge transfer process are considered. Severe solar activity can be harmful to spacecraft subsystems, causing electrical failures and differential charge driven arcing events, but consideration of these phenomena is beyond the scope of this paper [27]. For the moderate storm condition ($K_p = 6$), data from [24] are used to determine plasma temperatures and densities. The data are taken at a local time of 3:00, which corresponds to the postmidnight period where high natural charging is observed. For the severe storm condition, the plasma parameters corresponding to a severe storm in [39] are used. The ion and electron densities for both storm conditions are presented in Table I, along with the quiet ($K_p = 1.5$) conditions computed for 3:00 local time using the data in [24].

TABLE I
PLASMA PARAMETERS USED FOR GEOMAGNETIC STORM ANALYSIS

Storm Level	n_e (cm^{-3})	T_e (keV)	n_i (cm^{-3})	T_i (keV)
Moderate (K_p=6)	1	4.7	1	15
Severe (K_p=8-9)	1	20	1	20
Quiet (K_p = 1.5)	0.925	2.64	3.05	0.05

As Fig. 2 shows, storm events in GEO are relatively infrequent. In addition to solar storms, hot plasma may present in GEO during local substorms, which occur more frequently than solar storms [28]. During these substorms, electrons with energy levels below a few hundred kiloelectron-volts are injected into the inner magnetosphere, which can cause spacecraft charging. For the purposes of the analysis performed here, the distinction between solar storms and geomagnetic substorms is not of critical importance. Our goal is to identify the trends that result from hot plasma in the GEO environment. While there is certainly a significant amount of variability in GEO plasma conditions, the parameters in Table I are indicative of the conditions that may be present during storm/substorm events.

To determine the effects of storm conditions, the tug and debris potentials are computed as a function of electron beam current, for $E_{\rm EB} = 40$ keV, $r_T = 2$ m, and $r_D = 0.935$ m. The potentials are computed using the charge model presented in Section II-A, with the tug potential determined by (8) and the debris potential determined by the solution to (9). The electrostatic force is also computed, assuming a separation distance of 12.5 m. The potentials and forces are also computed for the quiet solar conditions ($K_p = 1.5$) to serve as a baseline for comparison. For the moderate solar storm event ($K_p = 6$), the results are shown in Fig. 6. Also shown are potentials computed using the quiet conditions. The storm conditions result in the tug charging to higher positive potentials for a given emitted electron beam current. For the debris, the maximum potential occurs at a lower beam current level, and the potential decreases at a faster rate as the beam current is increased. The tug reaches its maximum potential ($q\phi_T = E_{\rm EB}$) at a lower current level than for quiet space weather conditions. Considering the electrostatic forces that result, a slightly higher maximum force occurs for the storm condition and it occurs at a lower beam current level. The potentials and forces are also computed for the severe storm conditions and are shown in Fig. 7. The same effects are observed that are seen for moderate storm conditions, but to a higher degree. The tug potential increases more rapidly than during quiet conditions as beam current is increased, and the debris potential decreases in a similar fashion. For the severe storm condition, the tug reaches its maximum potential for a beam current of about 575 μA, while in the moderate storm condition, the tug potential is at its maximum for a beam current of almost 900 μA. As the storm severity increases, less current is required to maximally charge the tug (positive). Looking at the electrostatic forces for the severe storm condition, the maximum is once again slightly above that of the quiet condition, but occurs at much less current.

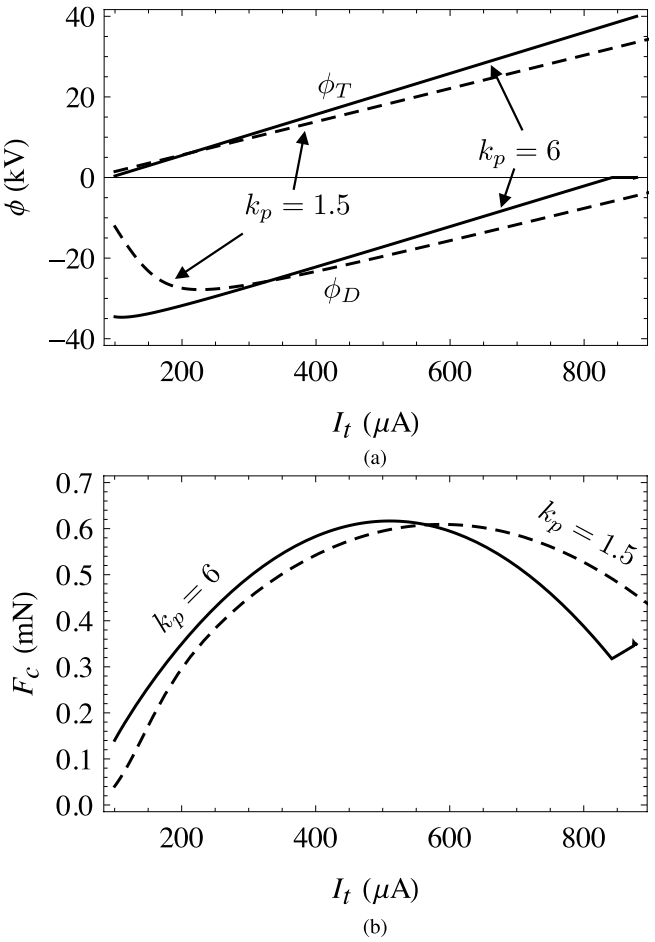

Fig. 6. (a) Potentials and (b) electrostatic force as a function of electron beam current for moderate solar storm event (solid lines and solid curves) and quiet solar conditions (dashed lines and dashed curves). The results assume $r_T = 2$ m, $r_D = 0.935$ m, and $E_{\rm EB} = 40$ keV.

Clearly, geomagnetic storm events do not prevent charge transfer for the electrostatic tractor. In fact, they are actually somewhat helpful. The increased electron temperature resulting from a storm event results in higher electron temperatures and thus higher momentum, making it more difficult for the positively charged tug to collect them. This reduces the plasma electron current collected by the tug for a given positive potential, driving the tug equilibrium potential in (7) to a higher value. A slightly higher electrostatic force is possible, and less current is required to achieve it. Current modification is required to compensate for the onset of these storm events, however. When considering the nominal GEO space weather conditions for quiet periods of activity, the maximum electrostatic force occurs for a beam current of nearly 600 μA. If a severe solar storm event occurs and the beam current is not modified to compensate for, Fig. 7 shows that the tug will reach its maximum potential ($q\phi_T = E_{\rm EB}$), preventing charge transfer and significantly impacting performance. Thus, to account for solar storm events, the beam current should be controllable, which is likely to be the case anyway. The analysis of solar storm events on tractor performance reveals that the worst case scenario from a performance perspective is actually the nominal quiet space weather conditions.

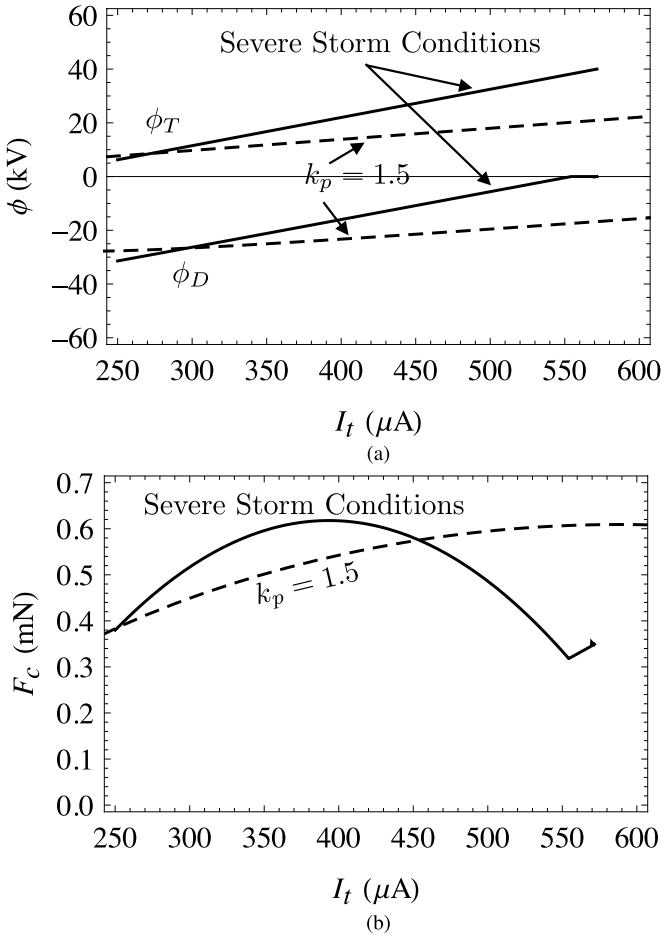

Fig. 7. (a) Potentials and (b) electrostatic force as a function of electron beam current for severe solar storm event (solid lines and solid curves) and quiet solar conditions (dashed lines and dashed curves). Results assume $r_T = 2$ m, $r_D = 0.935$ m, and $E_{\mathrm{EB}} = 40$ keV.

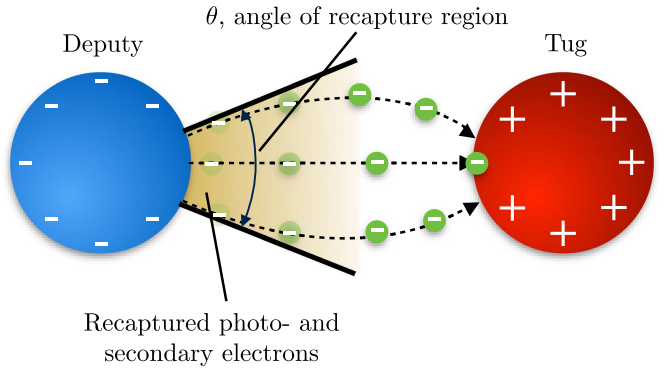

Fig. 8. Electron back flux from the debris to the tug.

For this reason, quiet storm conditions are assumed for further studies.

IV. Tug Electron Back Flux

Two debris current sources are due to emission of electrons from the debris surface: 1) photoelectron and 2) secondary electron emission. Because the debris is charged negatively, these electrons are lost. The nearby tug, however, recaptures a portion of these emitted electrons, as shown in Fig. 8, owing to high positive potential. This serves as an additional current source on the debris object which will impact its charging. Thus, it is important to study this effect and obtain a rough estimate for how significantly these current sources affect tug charging. The scope of this analysis is not meant to be comprehensive, but rather to provide some insight into how much this back flux might affect electrostatic tractor performance. A 2-m radius is assumed for both tug and debris and the quiet space weather conditions at 17:30 local time are used, corresponding to $n_e = 0.47$ cm^{-3}, $T_e = 1180$ eV, $n_i = 11$ cm^{-3}, and $T_i = 50$ eV [24]. These values are chosen to represent the worst case charge transfer performance conditions, as observed in [29].

To identify the angle of the recapture region, θ (see Fig. 8), the Nascap-2k spacecraft charging analysis software is used [40]. Developed by NASA and the Air Force Research Laboratory, Nascap-2k is capable of simulating charging behavior of 3-D spacecraft models, computing potentials in space and tracking particle trajectories. To identify the region of recapture, potentials are prescribed onto two spherical objects (each with 2-m radius) separated by a distance of 12 m. Nascap-2k is then used to compute the potentials in space around the objects. Following this computation, electrons are distributed around the debris object with a temperature of 2 eV. These electrons may represent either secondary or photoelectrons, as both are emitted at low energy. The electron trajectories are then computed to determine if they are recaptured by the tug vehicle. Two particular cases are considered: 1) $\phi_T = -\phi_D = 20$ kV and 2) $\phi_T = -\phi_D = 10$ kV.

The resulting electron trajectories are shown in Fig. 9. The region of recapture for the 10 and 20 kV equal potential cases is nearly identical, with $\theta = 20°$. Any electrons emitted within this region will be recollected by the tug, constituting an additional current source that will affect tug charging. If the electron beam is directed along the line of sight from tug to debris and is sufficiently narrow when it reaches the debris, a very large portion of the resulting secondary electrons may be recaptured by the tug. Depending on the potential levels of tug and debris, the secondary electron current can be a significant fraction of the beam current. To avoid the recapture of these electrons, a very narrow electron beam may not be the best choice. Alternately, the electron beam could be focused onto an area outside the region of recapture. It should be noted that the electron beam itself is not included in the Nascap simulation, and the beam electrons will have some effect on the recapture of the backscattered electrons. Here, a worst case scenario is considered where there is no interference from the electron beam, and a majority of the electrons in the recapture region are collected by the tug.

The back flux of photoelectrons is an additional current source onto the tug. Assuming a worst case scenario where the sun shines directly onto the region of recapture, the maximum cross-sectional area for which emitted photoelectrons are recaptured is

$$A_{\perp} = \pi r_D^2 \sin^2\left(\frac{\theta}{2}\right). \tag{16}$$

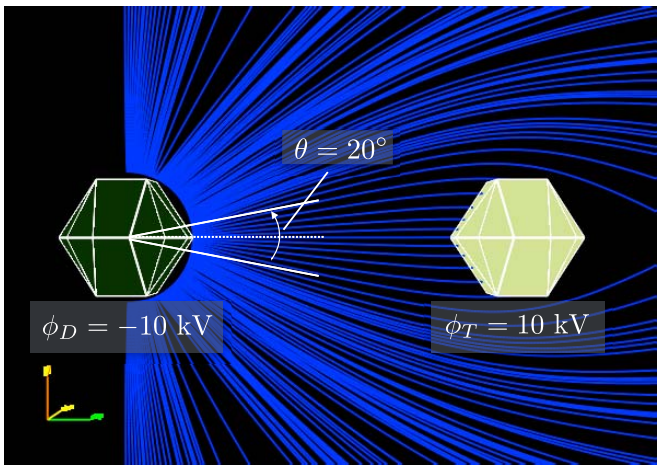

(a)

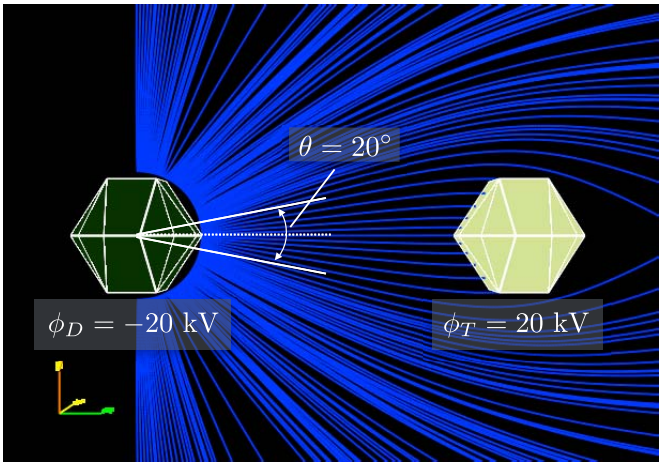

(b)

Fig. 9. Electron back flux trajectories computed by Nascap-2k for (a) $\phi_T = -\phi_D = 10$ kV and (b) $\phi_T = -\phi_D = 20$ kV. The results assume spheres of 2-m radius separated by a distance of 12 m.

For a physical description of the angle of recapture θ, the reviewer should consult Figs. 8 and 9. While potential is not contained explicitly in (16), it is implicit in θ because the tug and debris potentials do affect the region of recapture, which is characterized by θ. This is a higher area than could physically be exposed to sunlight because the tug would shadow at least some portion of the debris. Assuming the tug is at potential levels of at least a few kilovolts, the magnitude of this recaptured photoelectron current is insensitive to further increases in electron beam current. The recaptured photoelectron current is expressed as

$$I_{\text{ph,r}} = -\pi j_{\text{ph}} r_D^2 \sin^2\left(\frac{\theta}{2}\right). \tag{17}$$

To provide insight into how significant this current is on the tug, it is compared with the collected plasma electron current (I_e). Using the value of $\theta = 20°$ determined from the Nascap-2k simulations, the ratio of recaptured photoelectron current to plasma electron current is shown in Fig. 10. For the tug potentials considered for the electrostatic tractor application, the recaptured photoelectron current is a very small fraction (5% or less) of the incoming plasma electron current.

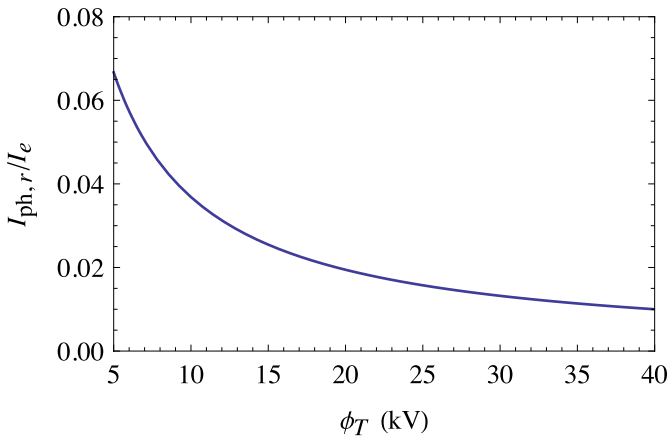

Fig. 10. Ratio of recaptured photoelectron current and tug plasma electron current for 2-m tug and debris radii.

Thus, this effect will not significantly impact the charging of the tug. The tug vehicle can simply emit slightly more current to offset these recaptured photoelectrons.

Assessing the impacts of recaptured secondary electrons is somewhat more complicated, because the recaptured secondary electron emission (SEE) current depends on how well focused the beam is and how much beam current is absorbed by the debris. Assuming a worst case scenario where all secondary electrons are recaptured by the tug, the potentials ϕ_T and ϕ_D are found by solving

$$I_t + I_e(\phi_T) - I_{\text{SEE}}(\phi_T, \phi_D) + I_{\text{ph},r} = 0 \tag{18a}$$

$$I_D(\phi_T, \phi_D) + I_e(\phi_D) + I_i(\phi_D) + I_{\text{SEE}}(\phi_T, \phi_D) + I_{\text{ph}} = 0. \tag{18b}$$

In the absence of back flux, the tug potential is not a function of the debris potential and can be solved directly. With back flux, however, the tug potential is a function of the debris potential due to the recaptured secondary electrons and these two current balance equations must be solved simultaneously for ϕ_T and ϕ_D. Considering the same 2-m radius tug and debris objects, at a separation distance of 12 m, the potentials as a function of electron beam current are computed and shown in Fig. 11. Also shown for comparison are the charging results if back flux is neglected (or nonexistent). With back flux, the tug and debris potentials both increase as the electron beam is increased. Without back flux, the tug potential increases linearly; the debris potential increases up to a certain point and then begins to decrease. The presence of back flux results in potential changes of several kilovolts. The tug potential is lower than without back flux, while the debris potential is higher. The resulting electrostatic forces are also shown in Fig. 11. For lower current values, the electrostatic force is reduced by the back flux. However, there is a certain current level beyond which the electrostatic force is higher with back flux than without it.

The recaptured electrons reduce the tug potential for a given electron beam current. This allows for more current to be sent to the debris at a higher energy level. The beam electrons lose less energy because the potential difference between tug and debris is reduced by the back flux. Because they arrive

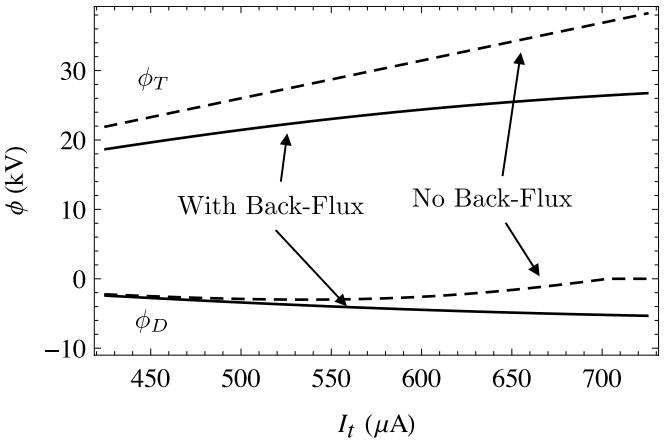

(a) Potentials

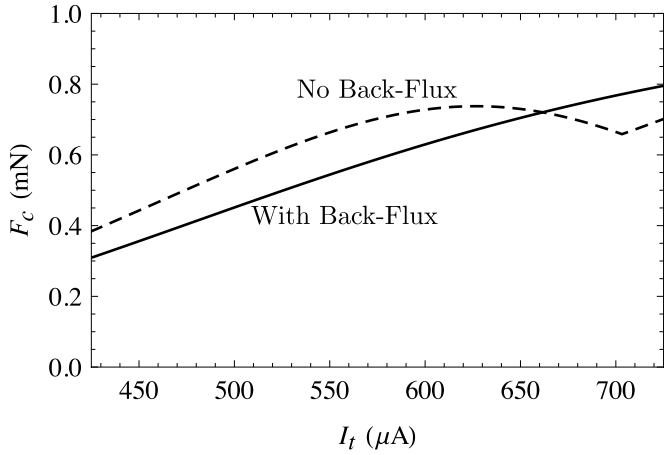

(b) Electrostatic Force

Fig. 11. (a) Tug and debris potentials with and without electron back flux onto the tug and (b) resulting electrostatic forces.

with more energy, the beam electrons induce fewer secondary electrons. This allows for the debris to reach a higher potential, which can improve tractor performance at the cost of higher electron beam current. This phenomenon is driven primarily by the recaptured secondary electrons, because this current source is significantly larger than the small portion of photoelectrons that are recaptured. Of course, this analysis assumes a worst case scenario where all secondary electrons emitted by the debris are recaptured by the tug, which depends on how well-focused the beam is and where it is absorbed on the debris. As a smaller portion of electrons are recaptured, the charging results approach those with no back flux.

V. Simultaneous Electron/Ion Beam Emission

Debris charging is limited by the amount of current that can be delivered to it by the tug. As the tug emits more electron beam current, it will charge itself to higher potentials. This results in the beam electrons having lower energy when they reach the debris, generally causing a higher secondary electron yield. Thus, the debris charging can actually decrease even for higher beam currents, as shown in Fig. 5. Furthermore, the plasma electron conditions can cause the tug to charge up to relatively high (positive) values and limit the debris potential. This can cause significant deviations from the ideal potential split, leading to reduced performance. These performance losses are encountered in the analysis of space weather variations on tugging performance studied in [29]. A dip in electron density after local noon results in a higher tug potential for a given beam current, which in turn results in a lower debris potential.

It would be very beneficial if the tug could change the amount of current delivered to the debris without affecting its own potential. If a tug vehicle could maintain, for example, a 20 kV potential while emitting a broad range of electron beam currents, debris charging could be improved and the tug vehicle would be able to perform charge transfer onto a wider variety of debris sizes. With only electron beam emission, of course, this is impossible. However, consider a scenario where the tug is equipped with not only an electron gun but also an ion beam. Assuming the ion beam is directed away from the debris object in a manner that does not result in an additional current source on the debris, the debris charging dynamics would be the same as in (9). Assuming there is sufficiently more electron beam current than ion beam current so that the tug charges to a high positive potential, the tug current balance takes on the slightly modified form

$$I_t - I_b + I_e(\phi_T) = 0 \tag{19}$$

where I_b is the ion beam current. Note that electron back flux is ignored here. This may be accomplished with a defocused electron beam or by focusing the electron beam away from the region of recapture. The tug potential, then, is a function of the net emitted current $\Delta I_B = I_t - I_b$

$$\phi_T = \left(\frac{4\Delta I_B}{Aqn_e w_e} - 1\right)\frac{k_B T_e}{q}. \tag{20}$$

The tug vehicle, being charged positive, will not recapture the beam ions in any significant capacity.

With the ion beam, a tug vehicle can theoretically emit any amount of electron beam current while maintaining a specific potential. For example, if the tug is desired to maintain a potential of 20 kV with a ΔI_B of 500 μA, any amount of electron beam current above 500 μA may be delivered to the debris. If 1000 μA of electron beam current is emitted, then 500 μA of ion beam current must also be emitted to maintain the necessary ΔI_B.

The ion beam emission allows for performance improvement in a variety of ways. Revisiting the issue of tug/debris size limitations, a tug would be able to achieve charge transfer onto objects larger than itself. With only an electron beam, the amount of beam current that the tug can emit is limited by the tug size. As the tug emits more current, it charges to a higher potential. The beam electrons that reach the debris have a lower effective energy when they arrive, resulting in further performance losses due to higher secondary electron emission. With an ion beam included, however, the tug can now deliver the necessary amount of electron beam current for debris charging. Emitting higher levels of electron beam current does not necessarily result in higher tug potentials, because ion beam current can be increased to maintain a constant tug potential. More current can be delivered to the debris at

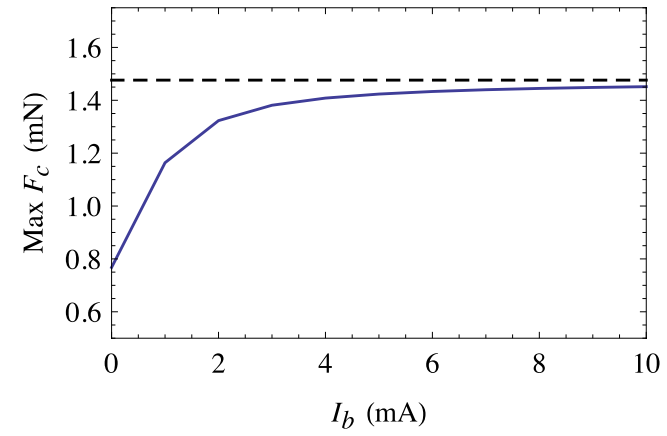

(a) Maximum E-Force

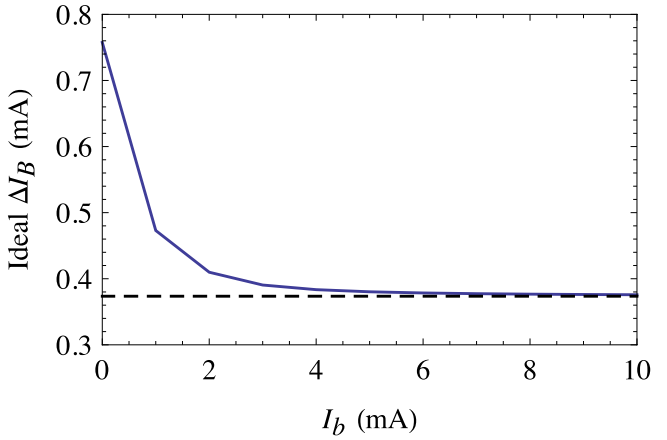

(b) Ideal ΔI_B

Fig. 12. (a) Maximum possible electrostatic force and (b) ΔI_B required to obtain the maximum force for simultaneous electron and ion beam emission. The dashed lines are the limiting values for the case of very large current emission. The results are computed with $r_T = r_D = 2$ m and $E_{\mathrm{EB}} = 40$ keV.

higher energies, inhibiting losses due to secondary electron emission. Considering the space weather driven performance losses encountered in [29], the increase in tug potential in the afternoon period can be eliminated by compensation with the ion beam. Keeping the tug potential from increasing also prevents the debris potential from decreasing. The end result is that both potentials remain close to the ideal split, where best performance occurs.

Naturally, simultaneous beam emission raises the question of what current emission strategy will yield the best performance for the electrostatic tractor. To provide insight into the effects of increasing electron and ion beam currents on the resulting electrostatic force, a numerical optimization is used. Considering a range of emitted ion beam currents, the maximum possible electrostatic force and its associated electron beam current are computed. The quiet GEO space weather conditions at 17:30 are again used. Both tug and debris are assumed to have radii of 2 m, and the electron beam energy is assumed to be 40 keV. The ion beam current is swept across a range of values, and the maximum possible electrostatic force is computed, along with the ΔI_B need to achieve the maximum force. The results are shown in Fig. 12. As the ion and, correspondingly, electron beam currents are increased, the maximum electrostatic force increases. However, there is a limit on the increase, regardless of how much current is emitted. This reflects the fact that for a given beam energy, the maximum potential difference between tug and debris is finite. Furthermore, as the current is increased, the ideal ΔI_B also converges toward a distinct value. Here, the inclusion of an ion beam allows for a significant boost in the electrostatic force magnitude. With only electron beam emission ($I_b = 0$), the maximum electrostatic force that can be generated is just under 0.8 mN. As the ion and, correspondingly, electron beam currents are increased, the maximum electrostatic force increases toward a limit of slightly less than 1.5 mN. This is an increase of 87%, which would nearly cut the reorbiting time required in half. It must be pointed out, however, that achieving this improved performance does require a significant increase in electron beam current. Increasing ever higher amounts current, especially at levels of tens of kilovolts, is difficult and will eventually be affected by the space charge limit. Thus, no assertion is made that the current levels considered here are necessarily possible; rather, we have identified that the ability to increase the electron beam current, even somewhat, with ion beam emission will improve tractor performance.

Clearly, though, there is a limit to how large of an electrostatic force may be generated, even for very high current levels. The only nonbeam debris current source that directly increases as a function of the electron beam current is the secondary electron current. As the beam current is increased to very high values, the ion and photoelectron currents become insignificant relative to the secondary electron and beam absorption currents. Thus, the debris will reach a potential that satisfies

$$I_D - 4Y_M I_D \kappa = 0. \tag{21}$$

Considering the case where the tug–debris potential difference is below the beam energy, this reduces to

$$1 - 4Y_M \kappa = 0. \tag{22}$$

Using the definition of κ in (6), the debris potential satisfies the equation

$$\begin{aligned} \phi_D = \phi_T - E_{\mathrm{EB}} + E_{\max}(2Y_M - 1) \\ + 2E_{\max}\sqrt{Y_M(Y_M - 1)}. \end{aligned} \tag{23}$$

The maximum secondary electron yield Y_M must be greater than one for a real solution to exist. In the case of a material with a maximum secondary yield below one, (23) is no longer valid to describe the debris potential and there is a discontinuity in the debris potential solution. If the secondary electron yield is always less than one, it is impossible for the secondary electron current to ever be of the same magnitude as the incoming electron beam current. Under this scenario, a different phenomenon drives the debris equilibrium potential. The debris potential will increase up to the point that there is no longer sufficient beam energy for the beam electrons to cross the potential difference between tug and deputy, resulting in the condition $q\phi_T - q\phi_D = E_{\mathrm{EB}}$.

The reader should keep in mind that the following results assume the maximum yield is greater than or equal to one. With simultaneous electron and ion beam emission, the largest theoretical difference that is possible between tug and debris is $E_{\rm EB} - E_{\max}\,(2Y_M - 1) + 2E_{\max}(Y_M(Y_M - 1))^{1/2}$. The losses in efficiency due to secondary electron emission are apparent.

To compute the maximum possible force with electron/ion beam emission, the charge product $q_T q_D$ extremum must be determined. Using (12) this product is simplified into the following cost function J by removing fixed parameters such as the sizes or separation distance that does not influence the extremum evaluation:

$$J = (r_D\phi_D - \rho\phi_T)(\rho\phi_D - r_T\phi_T). \tag{24}$$

Here, only the two potentials ϕ_D and ϕ_T are treated as unknown. After substituting in (23) for ϕ_D, and setting $\partial J/\partial\phi_T = 0$, the tug potential that will yield that maximum force is found to be

$$\phi_T^* = \frac{E_{\rm EB} - E_{\max}\left(2Y_M - 1 + 2\sqrt{Y_M(Y_M-1)}\,\right)}{2} \times \frac{\rho^2 - 2\rho r_D + r_D r_T}{(\rho - r_D)(\rho - r_T)}. \tag{25}$$

Similarly, the debris potential at the maximum force condition is

$$\phi_D^* = -\frac{E_{\rm EB} - E_{\max}\left(2Y_M - 1 + 2\sqrt{Y_M(Y_M-1)}\,\right)}{2} \times \frac{\rho^2 - 2\rho r_T + r_D r_T}{(\rho - r_D)(\rho - r_T)}. \tag{26}$$

The ΔI_B required to provide the necessary ϕ_T^* is

$$\Delta I_B^* = \frac{Aqn_e w_e}{4}\left(1 + \frac{q\phi_T^*}{k_B T_e}\right). \tag{27}$$

This limit is plotted in Fig. 12 for the scenario considered therein and reflects the asymptote that the numerically computed result is approaching. The theoretical maximum force that can be generated with both ion and electron beam emission is

$$F_c = -\frac{r_D r_T}{4k_c(\rho - r_D)(\rho - r_T)} \times \left(E_{\rm EB} + E_{\max}(1 - 2Y_M) - 2E_{\max}\sqrt{Y_M(Y_M-1)}\,\right)^2. \tag{28}$$

This limit is also plotted in Fig. 12, and the numerically computed maximum forces approach it as the currents are increased.

Of course, emitting arbitrarily large currents is not physically possible for a number of reasons. In addition to very high power requirements, the maximum current is limited by the space charge effect. If the charge density in a beam is high enough, the mutual repulsion between similarly charged particles reduces the beam velocity and limits the current flow [21]. These results should not be interpreted as implying that arbitrarily large currents can be emitted for the electrostatic tractor application. Rather, they serve to provide an upper limit on the performance improvement that may be gained by including ion beam emission in addition to electron beam emission. Further, Fig. 12 shows that for the vehicle sizes considered here, the achievable electrostatic forces with milliampere-level currents approach the theoretical maximum to within 10%. Electron beam currents in excess of 10 mA have been demonstrated in flight, and the SCATHA mission is one such example [41]. In the case of SCATHA, however, there was no need to focus the electron beam on another neighboring object, so beam expansion was not a concern. In the case of the electrostatic tractor, however, beam spreading requires more careful consideration because the concept depends on the ability to deliver the electron beam current to the debris object. Here, we have identified that ion beam emission has the potential to improve tractor performance by enabling the delivery of more beam current to the debris. However, emitting additional current introduces new challenges relating to the space charge limit and beam spreading, which are ripe areas for future work.

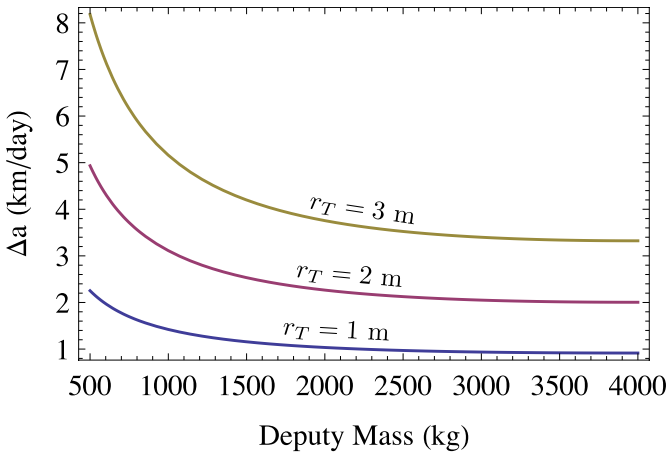

Fig. 13. Theoretical maximum semimajor axis increase per day for a range of tug and debris masses with simultaneous electron and ion beam emission. The results assume $E_{\rm EB} = 40$ keV.

The semimajor axis increases per day for a 1-, 2-, and 3-m radius tug as a function of debris mass are computed using the ideal electrostatic force expression in (28), assuming an electron beam energy of 40 keV and quiet space weather conditions at 17:30. The results are shown in Fig. 13. The largest 3-m radius tug provides the best performance, towing objects of 4000 kg with a semimajor axis increase of more than 3 km/day. For the 1-m tug, even simultaneous electron and ion beam emission is not enough to tow larger debris objects at a rate of $\Delta a = 1$ km/day.

Considering the dual beam scenario, we address the question of the maximum towable debris mass. To compute the maximum towable mass, the linear mass-radius relationship in (15) is employed. Using the best-case electrostatic force predicted by (28) in conjunction with the approximate semimajor axis increase per day from (14) allows for a numerical solution of the debris mass that will yield a desired Δa given a particular tug radius, separation distance, and electron beam energy. Two performance thresholds are used: $\Delta a = 1$ km and $\Delta a = 2.5$ km. The $\Delta a = 1$ km performance level is somewhat lower than typically assumed, and for the debris reorbiting

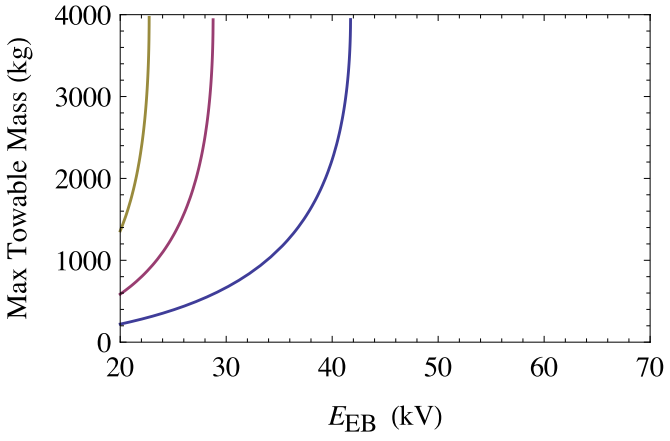

(a)

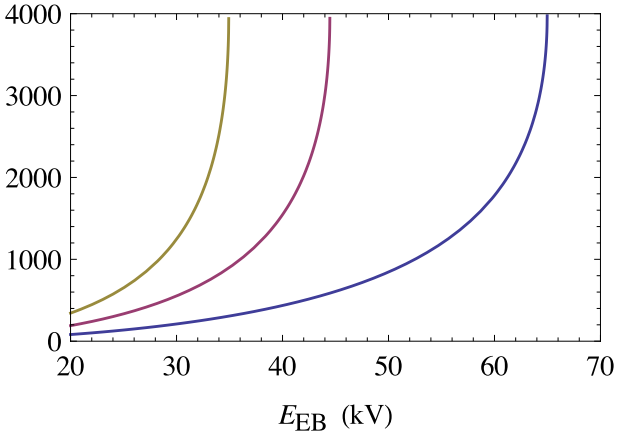

(b)

Fig. 14. Maximum towable mass using simultaneous electron and ion beam emission to meet performance criteria of (a) $\Delta a = 1$ km/day and (b) $\Delta a = 2.5$ km/day.

scenario would require a maneuver duration of roughly 7–10 months. The higher performance level of $\Delta a = 2.5$ km is more typical of what has been assumed in prior electrostatic tractor research [7].

The maximum towable masses as a function of electron beam energy are shown in Fig. 14 for tug sizes of $r_T = 1$, 2, and 3 m. The improved performance for larger tug vehicles is apparent. Significantly less beam energy is needed to achieve the same level of performance for the 3-m tug radius than for the 1-m tug radius. By incorporating ion beam emission, a tug with a 1-m radius can tow objects as large as 4000 kg at a rate of $\Delta a = 2.5$ km/day with an electron beam energy of 65 keV. To achieve a Δa of 2.5 km/day, the 3-m radius tug needs only 35 keV.

Ion beam emission, owing to the higher mass of ions relative to electrons, can impart a significant thrust force onto the tug vehicle. In fact, low-thrust propulsion systems have been designed around continuous ion emission [42]–[44]. Further, the ion beam shepherd concept considers the use of a collimated ion beam to impart a small force onto a debris object due to the impact of the incoming ions on the debris object, which is used for deorbiting purposes [45]. For the case of simultaneous ion and electron beam emission, performance

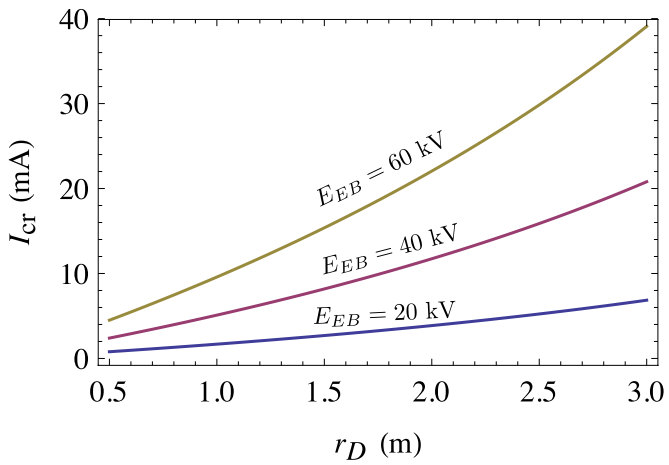

Fig. 15. Ion beam current for which F_{th} is equal to the maximum possible electrostatic force for simultaneous electron and ion beam emission.

improves as more beam current is emitted. Because the ion thrust force increases as more current is emitted, there will be a point beyond which the thrust force is higher than the electrostatic force. Because the tug vehicle is charged to a high positive potential ions that are emitted will be repelled, so there is no need for a high energy ion beam. It is assumed that the ions are emitted in a direction that will not lead to their capture by the negatively charged debris.

The thrust force on the tug due to the ion beam emission is

$$F_{\text{th}} = \frac{I_b}{q} m_b v_\infty(\phi_T) \tag{29}$$

where m_b is the mass of the ions and

$$v_\infty(\phi_T) = \sqrt{\frac{2q\phi_T}{m_b}} \tag{30}$$

is the velocity of the ions at infinity, after they have been accelerated out of the tug potential well. This formulation assumes that the ions are emitted with low energy, and that all of their v_∞ is due to acceleration by the tug's electric field. The ion species is assumed to be argon (Ar^+), with an associated mass of $m_b = 6.63 \times 10^{-26}$ kg. The thrust force matches the performance limit for dual beam emission when

$$\frac{I_b}{q} m_b v_\infty(\phi_T^*) = -\frac{r_D r_T}{4k_c(\rho - r_D)(\rho - r_T)} \times \left(E_{\text{EB}} + E_{\max}(1 - 2Y_M) - 2E_{\max}\sqrt{Y_M(Y_M - 1)}\right)^2. \tag{31}$$

Solving this equation for I_b yields the critical beam current I_{cr} for which more force is generated by the ion beam emission than is possible for the electrostatic attraction. Considering the case of a 2-m tug radius, this critical current level is computed for electron beam energies of 20, 40, and 60 keV and presented in Fig. 15. Higher beam energies allow for higher potentials on tug and debris, resulting in a larger electrostatic force. Thus, it takes more ion beam current to generate equivalent levels of thrust. As r_D is increased, more charge accumulates on the debris for the same potential level. This also results in

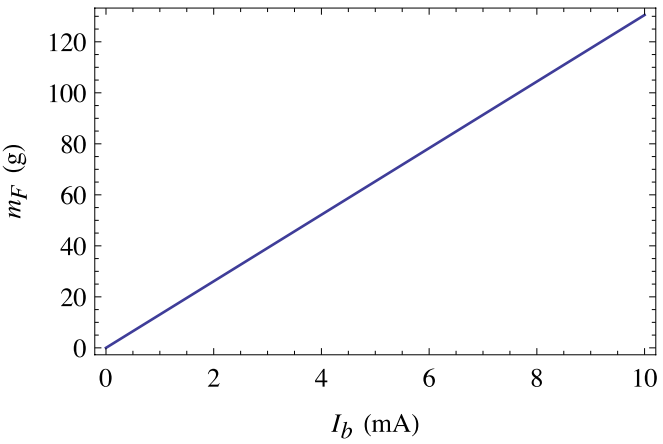

Fig. 16. Fuel required for continuous ion beam emission over the course of one year.

a larger electrostatic force and a higher $I_{\rm cr}$ level. Depending on $E_{\rm EB}$ and the debris size, only a few milliamperes of current are required for the ion beam thrust to equal the maximum electrostatic force. As observed in Fig. 12, it may take several milliamperes of current before the electrostatic force magnitude begins to closely approach the theoretical maximum. This implies that actually achieving the potential increases that are possible with dual beam emission may result in a scenario where the ion beam thrust is on the same order of the electrostatic force. Considering again the scenario shown in Fig. 12, with a 2-m tug and debris radius, the electrostatic forces begin to closely approach the theoretical maximum around an ion beam current of 5–6 mA. Considering Fig. 15, the amount of ion beam current required to reach the level of these electrostatic forces is 12 mA. For this particular scenario, where roughly 5–6 mA of ion beam current are required to achieve maximum performance, the thrust due to the resulting ion beam emission is roughly half of the electrostatic force magnitude.

Operating the ion beam requires a consumable source of fuel for ion generation. The reorbiting times of several months means that the ion beam will have to be emitted continuously for a long duration. Thus, it is of interest to investigate roughly how much fuel is required for ion beam operation. The mass flow rate of fuel due to the ion beam is computed as

$$\dot{m}_F = \frac{I_b}{q} m_i. \tag{32}$$

Considering a continuous operating time of one year, the total fuel consumption for a range of ion beam currents is shown in Fig. 16. For current levels of several milliamperes, the total fuel consumption is about 130 g. Considering the sizes of the tug and debris objects, this is a negligible increase in total system mass and not a significant hindrance for adding ion beam emission.

The decision to equip a tug vehicle with both an ion and electron beam depends on several factors. Really, maximizing the benefits that are possible with simultaneous emission requires a large increase in the emitted beam current levels. This has a direct impact on the resulting power requirements. For a 2-m tug with only an electron beam, the maximum power required for beam operation is driving the tug to its maximum potential ($q\phi_T = E_{\rm EB}$) and is about 30 W. Maximizing performance benefits with an ion beam requires at least several milliamperes of current. Estimating power requirements as $P = I_t E_{\rm EB}/q$, emitting 6 mA of electron beam current with an energy of 40 keV requires 240 W. This is an increase of 700%, and does not even include additional power consumption due to the ion beam emission. Still, power generation in excess of 10 kW has been achieved in operating GEO satellites [46], so this issue of increased power consumption is not likely to pose any significant technical hurdles.

Another practical concern is the additional complexity of adding a second current source (the ion beam). While it can greatly improve the performance for smaller tug vehicles where electron beam only charge transfer onto large debris objects fails, this must be weighed against the decision to simply build a larger tug vehicle with only an electron beam. Increasing the size of the tug does not necessarily necessitate increased vehicle mass and higher launch costs. There are no requirements on tug density, so it could be built like a hollow shell, keeping the mass increases manageable for larger tug vehicles.

Finally, the ion beam emission introduces a significant thrust force. While this does not preclude any functionality of the electrostatic tractor, it is something that the relative motion control system will have to compensate for, increasing the required thrust for station keeping. If the ions are emitted directly away from the debris object, a ion beam thrust on the same order as the electrostatic will double the station-keeping thrust requirements. This will, in turn, double fuel requirements. It may be possible, however, to mitigate these effects somewhat by emitting the ions such that they provide some portion of the required station-keeping thrust. Doing so, however, would require emission in the direction of the debris object. This could lead to recollection of the ions by the debris, which would reduce debris charging and hurt tractor performance. A full analysis of this phenomenon is beyond the scope of this paper.

VI. Conclusion

The impacts of geomagnetic storm activity on charge transfer for the electrostatic tractor application are considered. While the variations in the plasma environment resulting from these storm events do affect the charging of tug and debris, they can actually improve tractor performance. The tug must be able to compensate, however, by modifying electron beam current for the onset of such storms or performance will suffer. Both photoelectrons and secondary electrons are emitted from the debris in the near vicinity of the positively charged tug. Some of the electrons are recaptured by the tug, resulting in an additional current source. This back flux also somewhat improves tractor performance by allowing the tug to deliver more current at a slightly higher energy to the debris. Charge transfer performance can be improved by incorporating an ion beam onto a tug vehicle equipped with an electron beam. Simultaneous electron and ion beam emission allows the tug to deliver more electron current to the debris while keeping its own potential from increasing. This allows the debris to reach

a higher potential and the tractor force may be significantly improved, especially for smaller tug vehicles where charge transfer fails with only an electron beam. Of course, this comes at the cost of higher power requirements and the added complexity of dual-beam emission.

ACKNOWLEDGMENT

The authors would like to thank Z. Sternovsky for his input on the charging dynamics.

REFERENCES

[1] Swiss Reinsurance Company Ltd. (Mar. 2011). *Space Debris: On Collision Course for Insurers?* [Online]. Available: http://media.swissre.com/documents/Publ11_Space+debris.pdf

[2] P. V. Anderson and H. Schaub, "Local orbital debris flux study in the geostationary ring," *Adv. Space Res.*, vol. 51, no. 12, pp. 2195–2206, 2013. [Online]. Available: http://www.sciencedirect.com/science/article/pii/S0273117713000410

[3] P. V. Anderson and H. Schaub, "Local debris congestion in the geosynchronous environment with population augmentation," *Acta Astron.*, vol. 94, no. 2, pp. 619–628, Feb. 2014.

[4] Steering Group and Working Group 4, "IADC space debris mitigation guidelines," Inter-Agency Space Debris Coordination Committee, Houston, TX, USA, Tech. Rep. IADC-02-01, 2007.

[5] T. W. Wilcutt, "Process for limiting orbital debris," NASA, Washington, D.C., USA, Tech. Rep. NASA-STD-8719.14A, 2012.

[6] N. Murdoch, D. Izzo, C. Bombardelli, I. Carnelli, A. Hilgers, and D. Rodgers, "Electrostatic tractor for near earth object deflection," in *Proc. 59th Int. Astron. Congr.*, Glasgow, Scotland, 2008, paper IAC-08-A3.I.5.

[7] H. Schaub and D. F. Moorer, Jr., "Geosynchronous large debris reorbiter: Challenges and prospects," *J. Astron. Sci.*, vol. 59, nos. 1–2, pp. 165–176, 2012.

[8] E. A. Hogan and H. Schaub, "Relative motion control for two-spacecraft electrostatic orbit corrections," *J. Guid., Control, Dyn.*, vol. 36, no. 1, pp. 240–249, Jan./Feb. 2013.

[9] Y. S. Karavaev, R. M. Kopyatkevich, M. N. Mishina, G. S. Mishin, P. G. Papushev, and P. N. Shaburov, "The dynamic properties of rotation and optical characteristics of space debris at geostationary orbit," in *Proc. Adv. Astron. Sci.*, vol. 119. 2004, pp. 1457–1466, paper AAS-04-192.

[10] P. Couzin, F. Teti, and R. Rembala, "Active removal of large debris: Rendezvous and robotic capture issues," in *Proc. 2nd Eur. Workshop Active Debris Removal*, Paris, France, 2013, paper 7.5.

[11] L. B. King, G. G. Parker, S. Deshmukh, and J.-H. Chong. (Jan. 2002). "Spacecraft formation-flying using inter-vehicle Coulomb forces," NASA/NIAC, Tech. Rep. [Online]. Available: http://www.niac.usra.edu

[12] H. Schaub and D. Stevenson, "Prospects of relative attitude control using Coulomb actuation," in *Proc. Jer-Nan Juang Astrodyn. Symp.*, College Station, TX, USA, Jun. 2012, paper AAS 12-607.

[13] D. Stevenson and H. Schaub, "Multi-sphere method for modeling spacecraft electrostatic forces and torques," *Adv. Space Res.*, vol. 51, no. 1, pp. 10–20, Jan. 2013.

[14] P. Couzin, F. Teti, and R. Rembala, "Active removal of large debris: System approach of deorbiting concepts and technological issues," in *Proc. 6th Eur. Conf. Space Debris*, Darmstadt, Germany, Apr. 2013, paper 6a.P-17.

[15] A. Natarajan and H. Schaub, "Linear dynamics and stability analysis of a two-craft Coulomb tether formation," *J. Guid., Control, Dyn.*, vol. 29, no. 4, pp. 831–839, Jul./Aug. 2006.

[16] I. I. Hussein and H. Schaub, "Invariant shape solutions of the spinning three craft Coulomb tether problem," *J. Celestial Mech. Dyn. Astron.*, vol. 96, no. 2, pp. 137–157, 2006.

[17] S. Wang and H. Schaub, "Nonlinear charge control for a collinear fixed-shape three-craft equilibrium," *J. Guid., Control, Dyn.*, vol. 34, no. 2, pp. 359–366, Mar./Apr. 2011.

[18] H. Schaub and L. E. Z. Jasper, "Orbit boosting maneuvers for two-craft Coulomb formations," *J. Guid., Control, Dyn.*, vol. 36, no. 1, pp. 74–82, Jan./Feb. 2013.

[19] U. Yamamoto and H. Yamakawa, "Two-craft Coulomb-force formation dynamics and stability analysis with Debye length characteristics," in *Proc. AIAA/AAS Astrodyn. Specialist Conf. Exhibit*, Honolulu, HI, USA, Aug. 2008, paper AIAA 2008-7361.

[20] L. Felicetti and G. B. Palmerini, "Evaluation of control strategies for spacecraft electrostatic formation keeping," in *Proc. IEEE Aerosp. Conf.*, Big Sky, MT, USA, Mar. 2014, pp. 1–9, paper 2.0904.

[21] S. T. Lai, *Fundamentals of Spacecraft Charging: Spacecraft Interactions with Space Plasmas*. Princeton, NJ, USA: Princeton Univ. Press, 2012.

[22] T. Nakagawa, T. Ishii, K. Tsuruda, H. Hayakawa, and T. Mukai, "Net current density of photoelectrons emitted from the surface of the GEOTAIL spacecraft," *Earth, Planets Space*, vol. 52, no. 4, pp. 283–292, 2000.

[23] M. C. Kelley, *The Earth's Ionosphere: Plasma Physics & Electrodynamics*, vol. 96. San Diego, CA, USA: Academic, 2009.

[24] M. H. Denton, M. F. Thomsen, H. Korth, S. Lynch, J. C. Zhang, and M. W. Liemohn, "Bulk plasma properties at geosynchronous orbit," *J. Geophys. Res.*, vol. 110, no. A7, 2005.

[25] J. Bartels, N. H. Heck, and H. F. Johnston, "The three-hour-range index measuring geomagnetic activity," *J. Geophys. Res.*, vol. 44, no. 4, pp. 411–454, 1939. [Online]. Available: http://dx.doi.org/10.1029/TE044i004p00411

[26] (Mar. 2005). "NOAA space weather scales," Nat. Oceanic Atmos. Admin., Boulder, CO, USA, Tech. Rep. [Online]. Available: http://www.swpc.noaa.gov/noaa-scales-explanation

[27] H.-S. Choi *et al.*, "Analysis of GEO spacecraft anomalies: Space weather relationships," *Space Weather*, vol. 9, no. 6, 2011. [Online]. Available: http://dx.doi.org/10.1029/2010SW000597

[28] M. F. Thomsen, M. G. Henderson, and V. K. Jordanova, "Statistical properties of the surface-charging environment at geosynchronous orbit," *Space Weather*, vol. 11, no. 5, pp. 237–244, 2013. [Online]. Available: http://dx.doi.org/10.1002/swe.20049

[29] E. A. Hogan and H. Schaub, "Space weather influence on relative motion control using the touchless electrostatic tractor," in *Proc. AAS/AIAA Spaceflight Mech. Meeting*, Santa Fe, NM, USA, Jan. 2014, paper AAS 14-425.

[30] E. A. Hogan and H. Schaub, "Impacts of tug and debris sizes on electrostatic tractor charging performance," *Adv. Space Res.*, vol. 55, no. 2, pp. 630–638, Jan. 2015.

[31] H. Schaub and Z. Sternovsky, "Active space debris charging for contactless electrostatic disposal maneuvers," *Adv. Space Res.*, vol. 43, no. 1, pp. 110–118, 2014.

[32] R. Hippler, S. Pfau, M. Schmidt, and K. H. Schoenbach, Eds., *Low Temperature Plasma Physics: Fundamental Aspects and Applications*. Berlin, Germany: Wiley, 2001.

[33] B. T. Draine and E. E. Salpeter, "On the physics of dust grains in hot gas," *Astrophys. J.*, vol. 231, pp. 77–94, Jul. 1979.

[34] J. A. Bittencourt, *Fundamentals of Plasma Physics*. New York, NY, USA: Springer-Verlag, 2004.

[35] C. R. Seubert, L. A. Stiles, and H. Schaub, "Effective Coulomb force modeling for spacecraft in Earth orbit plasmas," *Adv. Space Res.*, vol. 54, no. 2, pp. 209–220, 2014. [Online]. Available: http://www.sciencedirect.com/science/article/pii/S0273117714002191

[36] S. E. DeForest, "Spacecraft charging at synchronous orbit," *J. Geophys. Res.*, vol. 77, no. 4, pp. 651–659, 1972. [Online]. Available: http://dx.doi.org/10.1029/JA077i004p00651

[37] S. J. Bame *et al.*, "Magnetospheric plasma analyzer for spacecraft with constrained resources," *Rev. Sci. Instrum.*, vol. 64, no. 4, pp. 1026–1033, 1993.

[38] E. G. Mullen, M. S. Gussenhoven, D. A. Hardy, T. A. Aggson, B. G. Ledley, and E. Whipple, "SCATHA survey of high-level spacecraft charging in sunlight," *J. Geophys. Sci.*, vol. 91, no. A2, pp. 1474–1490, 1986.

[39] M. J. Mandell, I. Katz, G. W. Schnuelle, P. G. Steen, and J. C. Roche, "The decrease in effective photocurrents due to saddle points in electrostatic potentials near differentially charged spacecraft," *IEEE Trans. Nucl. Sci.*, vol. 25, no. 6, pp. 1313–1317, Dec. 1978.

[40] M. J. Mandell, V. A. Davis, D. L. Cooke, A. T. Wheelock, and C. J. Roth, "NASCAP-2k spacecraft charging code overview," *IEEE Trans. Plasma Sci.*, vol. 34, no. 5, pp. 2084–2093, Oct. 2006.

[41] S. T. Lai, "An overview of electron and ion beam effects in charging and discharging to spacecraft," *IEEE Trans. Nucl. Sci.*, vol. 36, no. 6, pp. 2027–2032, Dec. 1989.

[42] D. M. Goebel and I. Katz, *Fundamentals of Electric Propulsion: Ion and Hall Thrusters*, vol. 1. New York, NY, USA: Wiley, 2008.

[43] J. R. Beattie, "Electrostatic ion thruster with improved thrust modulation," U.S. Patent 4 838 021, Jun. 13, 1989.

[44] P. J. Wilbur, V. K. Rawlin, and J. R. Beattie, "Ion thruster development trends and status in the United States," *J. Propuls. Power*, vol. 14, no. 5, pp. 708–715, 1998.

[45] C. Bombardelli and J. Peláez, "Ion beam shepherd for contactless space debris removal," *J. Guid., Control, Dyn.*, vol. 34, no. 3, pp. 916–920, May/Jun. 2011.

[46] C. F. Hoeber, I. Katz, V. A. Davis, and D. B. Snyder, "Solar array augmented electrostatic discharge in GEO," in *Proc. 17th AIAA Int. Commun. Satellite Syst. Conf. Exhibit*, Yokohama, Japan, Feb. 1998, paper AIAA 98-1401.

Erik A. Hogan was born in West Palm Beach, FL, USA, in 1986. He received the B.S. degree in aerospace engineering from the University of Central Florida, Orlando, FL, USA, in 2009, and the Ph.D. degree in aerospace engineering from the University of Colorado Boulder, Boulder, CO, USA, in 2014.

He served as a lead Graduate Teacher with the Department of Aerospace Engineering, University of Colorado Boulder, from 2012 to 2013. He has been a Dynamics and Controls Engineer with Space Systems Loral, Palo Alto, CA, USA, since 2014. He has authored over ten journal articles. His current research interests include dynamics and control of large, multibody flexible space structures, orbital debris mitigation, and the use of electrostatic forces for relative orbital motion control.

Dr. Hogan was a recipient of the Vela Fellowship to attend the Los Alamos Space Weather Summer School in 2012, the John V. Breakwell Student Travel Student Travel Award from the American Astronautical Society, and the Graduate Assistance in Areas of National Need Fellowship.

Hanspeter Schaub received the B.S., M.S., and Ph.D. degrees from Texas A&M University, College Station, TX, USA, in 1992, 1994, and 1998, respectively.

He was the Alfred T. and Betty E. Look Professor of Engineering and is currently with the Department of Aerospace Engineering Sciences, University of Colorado Boulder, Boulder, CO, USA. His 19 years of professional interests are in nonlinear dynamics and control applications, with a special emphasis on astrodynamics. He has performed research on spacecraft attitude and control, exploiting nonlinear dynamics of control moment gyros to avoid classical CMG singularities, and extensive research on spacecraft formation flying dynamics and control problems. His prior work experience includes four years with Sandia National Laboratories, Intelligent Systems and Robotics Center, and four years with the Department of Aerospace and Ocean Engineering, Virginia Tech, Blacksburg, VA, USA, as an Assistant Professor. He has authored about 106 peer-reviewed papers, presented over 150 conference papers, published a third edition text book in analytical mechanics of space systems, and holds patent in a noncontact position and orientation measurement system, and two patents in a touchless GEO debris reorbiting method. His current research interests include charged relative motion dynamics and control, space debris mitigation, three-axis attitude control, and visual servoing of autonomous vehicles.

Dr. Schaub is an Associate Fellow of the American Institute of Aeronautics and Astronautics and a fellow of the American Astronomical Society. He has received the H. Joseph Smead Fellow from the University of Colorado, the Provost's Faculty Achievement Award, the College of Engineering Outstanding Faculty Advisor Award, the Boulder Faculty Assembly Excellence in Teaching Award, and the Dean's Award for Outstanding Teaching. His textbook was a recipient of the AIAA Summerfield Book Award in 2013.